Product Study of the Photolysis of Ketene and Ethyl Ethynyl Ether at 193.3 nm

Christopher Fockenberg*

Chemistry Department 555A, Brookhaven National Laboratory, P.O. Box 5000, Upton, New York 11973-5000

Received: December 28, 2004; In Final Form: June 6, 2005

The product distributions of the excimer laser photolysis of ketene (CH_2CO) and ethyl ethynyl ether (C_2H_5-OCCH) at $\lambda = 193.3$ nm (ArF) were studied using a time-of-flight mass spectrometer (TOFMS) as an analytical tool. Ketene was photolyzed in bath gases consisting of mixtures of He and H_2/D_2 at various mixing ratios at constant total pressures of 4 Torr and temperature of about 300 K. Singlet methylene ($^1CH_2$) produced in the photolysis of ketene was almost instantaneously converted either to triplet methylene ($^3CH_2$) or to methyl radicals in collisions with He and H_2 or D_2. By extrapolating the methyl and methylene signals to zero time after photolysis, initial concentrations of these radicals were obtained. Analyzing the initial $^3CH_2$ and CH_3 concentrations as functions of hydrogen-to-helium ratios as well as simulating the observed traces of reactant and product species resulted in $^1CH_2 + CO$ (66 ± 8)%, as the main product channel of the ketene photolysis with smaller contributions from HCCO + H (17 ± 7)% and $^3CH_2 + CO$ (6 ± 9)%. Hydrogen atoms, acetylene, ethylene, ethyl, and ketenyl radicals, and small amounts of ketene were observed as primary products of the ethyl ethynyl ether photolysis. Quantification of C_2H_2, C_2H_4, C_2H_5, and CH_2CO product leads to a HCCO yield of (91 ± 14)%.

1. Introduction

The ArF excimer laser photolysis ($\lambda = 193.3$ nm) of ketene and ethyl ethynyl ether was studied as a source for ketenyl, HCCO radicals. Reactions of these radicals are of interest in combustion systems for various reasons. HCCO radicals are predominantly produced in the reaction of oxygen atoms with acetylene and can be converted in reactions with hydrogen atoms to singlet methylene, which in turn can react with acetylene, giving propargyl radicals, a precursor in the formation of soot.[1] HCCO is also implicated as the main reducing agent for nitric oxide, NO, in the NO_x-reburn mechanism.[2] To investigate reactions of ketenyl radicals experimentally, ketene has been used predominantly as a precursor species for ketenyl radicals in the past.[3,4] However, HCCO + H is only a minor product channel (< 20%) in this process.[4,5] The main products are CH_2 + CO, which can render product studies of HCCO reactions challenging because of interfering reactions involving methylene radicals. An example would be the HCCO + O_2 reaction, which was recently investigated by Osborn.[6] Because HCCO as well as CH_2 produce CO and CO_2 in reactions with O_2,[7] it would have been difficult to distinguish between these two sources and determine exact product yields. However, Osborn used ethyl ethynyl ether (EEE) instead, which has been shown in a photodissociation dynamics study to give HCCO in quantum yields close to unity at 193 nm.[8] To provide an independent determination of the EEE photolysis products, as well as to clarify conflicting results for the ketene photolysis, in particular, with respect to the electronic state (singlet or triplet) of the methylene radicals produced, photolysis products of both precursors were studied in this work.

For ethyl ethynyl ether, many product channels are energetically possible, and only those considered in this work are mentioned below. Reaction enthalpies were calculated with heats of formation from Table 1, including 618.9 kJ/mol deposited in the molecule after absorbing a 193.3-nm photon.

TABLE 1: Enthalpies of Formation at 298 K (kJ/mol)

	$\Delta_f H°_{gas}$	reference
CH_2CO	−49.58	45
$C_2H_5OC_2H$	72.4	8
HCCO	176.6	46
$^3CH_2$ ($\tilde{X}\ ^3B_1$)	390.41	45
$^1CH_2$ ($\tilde{a}\ ^1A_1$)	428.07	45
$^1CH_2$ ($\tilde{b}^1B_1$)	528	23
CH_3	146.65	45
H	218	47
C_2H_2	226.73	47
C_2H_4	52.47	47
C_2H_5	119	48
CO	−110.53	47
C_2O	286.60	47
CH_3CHO	−170.7	49

$$C_2H_5OCCH + h\nu \rightarrow C_2H_5 + HCCO \quad \Delta H°\,(298\ K, kJ/mol) = -395.6 \quad (R1a)$$

$$\rightarrow C_2H_4 + CH_2CO \quad \Delta H°\,(298\ K, kJ/mol) = -688.3 \quad (R1b)$$

$$\rightarrow C_2H_4 + H + HCCO \quad \Delta H°\,(298\ K, kJ/mol) = -244.2 \quad (R1c)$$

$$\rightarrow C_2H_2 + CH_3CHO \quad \Delta H°\,(298\ K, kJ/mol) = -635.2 \quad (R1d)$$

It is noteworthy that, for some cases, the exothermicity is large enough to allow secondary decomposition of internally excited products.

Krisch et al. measured the dynamics of the 193-nm photodissociation of EEE in a molecular beam using synchrotron radiation or electron bombardment to ionize the fragments.[8]

* Corresponding author. E-mail: christopher.fockenberg@web.de.

10.1021/jp044092g CCC: $30.25
Published on Web 07/22/2005

HCCO radicals were found to be vibrationally and electronically excited. Other than C_2H_5, no other products (mass channels associated with C_2H_2, CH_3CHO, C_2H, and CH_2CO were probed) could be detected. No attempt was made to detect C_2H_4 because of the large background signal at mass 28. Thus, it was concluded that R1a is the only important channel for the photolysis of EEE.

For the ketene photolysis, several product channels are energetically possible, e.g.:

$$CH_2CO + h\nu \rightarrow CH_2\ (\tilde{b}\ ^1B_1) + CO \qquad \Delta H^\circ\ (298\ K, kJ/mol) = -151.8 \quad (R2a)$$

$$\rightarrow CH_2\ (\tilde{a}\ ^1A_1) + CO \qquad \Delta H^\circ\ (298\ K, kJ/mol) = -251.7 \quad (R2b)$$

$$\rightarrow CH_2\ (\tilde{X}\ ^3B_1) + CO \qquad \Delta H^\circ\ (298\ K, kJ/mol) = -289.4 \quad (R2c)$$

$$\rightarrow HCCO + H \qquad \Delta H^\circ\ (298\ K, kJ/mol) = -174.7 \quad (R2d)$$

$$\rightarrow C_2O + H_2 \qquad \Delta H^\circ\ (298\ K, kJ/mol) = -282.7 \quad (R2e)$$

Again, the reaction enthalpies were calculated with heats of formation from Table 1 with 618.9 kJ/mol added.

Ketene is initially excited to a $^1B_1$ state by absorption of a 193-nm photon correlating to the CH_2 ($\tilde{b}\ ^1B_1$) + CO product channel,[9,10] which is consistent with observations made by Ruiz and Martín, who studied fluorescence signals after photolysis of ketene at 193.3 nm.[11] The emission was attributed to the $^1B_1 \rightarrow {}^1A_1$ transition in CH_2 with an overall fluorescence lifetime of less than 10 μs at a few mTorr of ketene; efforts to detect CH_2 ($\tilde{a}\ ^1A_1$) by laser-induced fluorescence were unsuccessful. Glass et al. photolyzed ketene in mixtures of H_2 and Ar (2−20 Torr, 298 K) and used atomic resonance absorption spectrometry to observe hydrogen atoms generated directly by the photolysis or in subsequent reactions.[5] They concluded that the CH_2 + CO channels have a combined yield of about 82% with R2c about three times more likely than R2b. No distinction between channels R2a and R2b was made because it was assumed that CH_2 ($\tilde{b}\ ^1B_1$) would be rapidly converted into CH_2 ($\tilde{a}\ ^1A_1$). R2d and R2e were reported to have similar yields with 10.7% and 7.2%, respectively. Feltham et al. studied the speed distribution of H atoms generated in the photodissociation of ketene at various UV wavelengths, including 193 nm.[12] In addition, RRKM calculations were performed to explain the kinetic energy release as well as internal energy distribution of the CO fragment, which was compared to data published by Fujimoto et al.[13] The authors concluded that only the $^1A_1$ ground potential energy surface of ketene was involved in the dissociation process and that $^1B_1$ ketene is converted quickly to the ground state via radiationless processes. The estimated yields for channels R2b and R2d are roughly 65% and 35%, respectively. Rim and Hershberger measured the total CO yield of the ketene photolysis at 296 K in bath gas mixtures of Xe and SF_6 at low pressures using IR diode laser absorption. The CO yield of 83% leaves a maximum yield of 17% for HCCO.[4]

In this paper, results will be presented from investigations of the product distribution of the ethyl ethynyl ether and ketene photolysis at 193 nm at temperatures around 300 K. To estimate the amount of radicals that can be produced in the photolysis of EEE, its absorption spectrum was taken between 155 and 220 nm. EEE was photolyzed mostly in helium as buffer gas at 4 Torr. In two experiments, helium was replaced by H_2 or D_2 in an attempt to capture HCCO radicals, a reaction for which the rate constant has recently been measured.[3] By quantifying several C2 product species (C_2H_2, C_2H_4, C_2H_5), the HCCO yield could be obtained.

Ketene was photolyzed in bath gases of mixtures of helium and hydrogen (H_2 or D_2) with varying mixing ratios at total pressures of 4 Torr. Following the same idea of Glass et al., singlet methylene either is rapidly deactivated to triplet methylene in collisions with the bath gas or is converted to methyl radicals (CH_3, CH_2D, or CHD_2) in reactions with H_2 or D_2. Because the detection method employed here is not state selective, the question as to whether $^1B_1$ or $^1A_1$ CH_2 is produced could not be answered. Interestingly, Hartland et al. suggested that the reactivity of $^1B_1$ CH_2 might be larger than that of $^1A_1$ CH_2, which would favor chemical reaction over deactivation by H_2 or D_2 here.[14] However, the lifetime of any $^1B_1$ methylene produced was considered very short, so that it was not necessary to invoke $^1B_1$ CH_2 in the data analysis, as will be shown below. Therefore, singlet methylene will be considered to be $\tilde{a}\ ^1A_1$ CH_2, while triplet methylene will denote $\tilde{X}\ ^3B_1$ CH_2 from here on. Triplet methylene and methyl radicals were observed directly as well as their reaction products. Analysis of the methylene-to-methyl ratios as a function of the hydrogen-to-helium mixing ratio produced the singlet and triplet methylene yields. The HCCO signal observed could be quantified using the results from the EEE photolysis.

2. Experimental Section

The experiments were performed in a flow reactor/repetitive sampled time-of-flight mass spectrometer (TOFMS) apparatus, which will be briefly discussed below. A detailed description can be found elsewhere.[15] The tubular quartz reactor (1-cm diameter) was coated with boric acid on the inside to reduce surface reactions. The temperature inside the tube was measured with thin-wire thermocouples. The content of the reactor was sampled continuously through a pinhole in the wall. A portion of the sampled gas was photoionized by the VUV radiation emitted from a hollow cathode lamp (McPherson, Model 630) operated with hydrogen as discharge gas. Isolating the lamp from the vacuum chamber by differential pumping of the connecting glass tube allowed windowless operation, which enabled the use of the whole H_2 emission spectrum for ionization. By switching voltages on the collection grid assembly at a high rate, "snapshots" of the composition of the reaction mixture can be taken; here, in intervals of 48 μs.

The radical precursors were photolyzed by the radiation of an ArF excimer laser (Lambda Physik, COMPEX 205), creating a homogeneous distribution of radicals along the tube. Intensities inside the reactor tube were usually less than 50 mJ/cm^2 per pulse. The laser intensity entering and exiting the reactor was monitored separately with two thermoelectric energy meters (Molectron J50). Mass spectra were summed typically for several tens of thousands of laser shots per experiment.

Mass-flow controllers (Tylan General, FC 260) were used to prepare the gas mixtures introduced into the reactor tube. Acetone (Mallinckrodt, 99.7%), 1,3-^{13}C-acetone (Cambridge Isotope Laboratories, ^{13}C-atom 99%), as well as all other liquid sources, were degassed in several freeze−pump−thaw cycles before use and stored as diluted mixtures in helium in 20-L glass vessels. Ethyl ethynyl ether (Aldrich, ∼40 wt % in hexanes) could be concentrated somewhat by pumping away half of the sample upon melting after the last freeze−pump−

thaw cycle. The remaining liquid was about twice as concentrated in ethyl ethynyl ether as the original. He (Welco CGI Gas Technologies, UHP grade) was used directly from the tank, whereas H_2 (Matheson, purity 99.9999%) and D_2 (Matheson, $\geq$ 99.7%, main impurities were CO and N_2) were passed through a cold trap at LN_2 temperature to remove traces of water. Ketene was produced in the pyrolysis of acetic acid anhydride (Aldrich, 99.5%) in a heated quartz tube filled with quartz beads. For this procedure, a controlled flow of helium was bubbled through a bubbler filled with acetic acid anhydride. The bubbler was placed in a water−ice slush bath to reduce the vapor pressure of the acetic acid anhydride. Before mixing the ketene/He flow with the other components, remaining acetic acid anhydride as well as water was trapped in a U tube, which was placed in an ethanol−dry ice slush. Mass spectra taken with hydrogen or neon as discharge gas in the hollow cathode lamp did not show any significant signals other than those associated with ketene, so that impurities did not have to be taken into account. The concentration of ketene could be changed either by adjusting the flow of helium or by changing the temperature inside the quartz tube. The pressure in the flow reactor was controlled by throttling the gas flow through a gate valve at the downstream end of the reactor. The flow velocity employed here was 8 m/s to minimize the pressure drop along the tube.

Typical concentrations in the reactor were $(4-8.5) \times 10^{12}$ molecules cm^{-3} of acetone, $(0.9-5) \times 10^{13}$ molecules cm^{-3} of ketene, and $(2.5-8) \times 10^{12}$ molecules cm^{-3} of ethyl ethynyl ether. Dependent on laser fluence and absorption coefficient, 2−8% of the precursor species was photolyzed per laser shot. Hydrogen concentration was varied in the ketene experiment between 1×10^{14} and 1.2×10^{17} molecules cm^{-3}.

For reference measurements, mixtures of C_2H_2 (Matheson, with acetone removed by LN_2/dry ice distillation), C_2H_4 (Matheson, >99%), C_2H_6 (Linde, > 99%), CH_3OH (Mallinckrodt), hexane (Aldrich >95%), hexanes (J. T. Baker), 3-pentanone (Fluka, >99.5%), CO (Matheson, >99%), and O_2 (Liquid Carbonic) with He were prepared in 3-L glass bulbs. Ketene was prepared as described above and frozen out in a cold trap at liquid nitrogen temperature. The trap was then placed in a dry ice/ethanol bath, after which the evaporated ketene was collected in a 3-L glass bulb and pressurized with helium.

The VUV absorption spectrum of EEE was taken with a McPherson Model 218 (0.3 m) vacuum scanning monochromator fitted with a 2400 grooves/mm grating (1500 Å blaze wavelength). No difference in the spectra could be detected for slit widths of 50 and 80 μm. The monochromator was evacuated by a McPherson 815 pumping control system. A deuterium lamp (Hamamatsu L7292) served as the light source. The windows of the glass sample cell ($l = 8.9$ cm) were MgF_2. Photomultipliers (EMI 9558), sample holder, and electronics were furnished by Acton Research Corporation. The sample holder featured a beam splitter in front of the sample cell, which directed a fraction of the VUV light onto a second photomultiplier for reference measurements of the initial intensity. A LabVIEW program controlled scan parameters and data acquisition via data acquisition boards. The scan speed was 2 nm per minute; signals were averaged for 3 or 1.5 s, giving a data point every 0.1 or 0.05 nm, respectively. The monochromator was calibrated by taking absorption spectra of SO_2 and comparing the peak positions between 190 and 220 nm to literature data,[16,17] which led to shifting the raw spectrum to shorter wavelengths by 0.615 nm. The overall wavelength accuracy is about $\pm$0.1 nm.

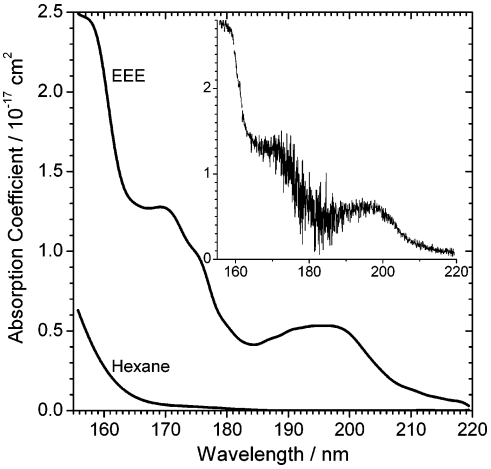

Figure 1. Absorption coefficients of ethyl ethynyl ether and hexane. The EEE spectrum is a smoothed average of three measurements with different EEE concentrations. The inset shows an original data set with 0.14 Torr of EEE/hexanes in 76 Torr of helium at 295 K. The EEE-to-hexanes ratio was 2.9, determined with the TOFMS apparatus. The high noise level between 170 and 190 nm is caused by the low intensity of the D_2 lamp in this range.

3. Data Analysis

Absorption Cross Section of Ethyl Ethynyl Ether. Absorption spectra were taken from samples of mixtures of EEE/hexanes in He as well as hexane in He at various pressures. The EEE/hexanes samples were taken from the same mixture that was used in the photolysis experiments. As will be described below, the EEE-to-hexanes ratio was determined by comparing the mass spectra of the EEE/hexanes mixture to mass spectra of known quantities of either neat hexane or hexanes. The absorption spectrum of EEE was obtained by subtracting the hexanes contribution from the acquired spectrum of the mixture. As can be seen in Figure 1, EEE has broad absorption features in the VUV, with an absorption cross section of σ (193.3 nm) $= (5.3 \pm 1.0) \times 10^{-18}$ cm^2 at 295 K. This value is about 25% lower than the one quoted by Osborn;[6] however, the lower value fits better with fractional drops observed with the time-of-flight apparatus for precursor species such as SO_2 and acetone after photolysis. In a previous publication, it was shown that the fractions of precursors photolyzed were proportional to the absorption coefficients.[18] SO_2 having the largest absorption cross section ($\sigma \approx 7 \times 10^{-18}$ cm^2) showed the largest drop, followed by EEE (~80% that of SO_2), followed by acetone (~50% that of SO_2, σ (acetone) $\approx 3.1 \times 10^{-18}$ cm^2)[19] and ketene (15% that of SO_2, σ (ketene) $\approx 1 \times 10^{-18}$ cm^2)[20] at the same excimer laser intensity.

Ethyl Ethynyl Ether Photolysis. To determine the product yields of each photolysis channel, the initial EEE concentration had to be known. For this purpose, the mass spectra of the EEE/hexanes mixtures were compared to mass spectra of either neat hexane or mixtures of hexanes (see Figure 2). Because there were only minor differences in fragmentation patterns or signal strengths between the spectra of hexane and hexanes, both compounds could be used as valid references. Peaks at masses 29, 55, and 70 could be attributed to EEE alone, while masses 56, 57, and 86 were purely hexanes, which also contributed about 6% to the peak at mass 42 in the EEE/hexanes mixture. The remaining 94% could be attributed to fragmentation of EEE after ionization. The hexanes fraction in the two dilute mixtures in helium used in the photolysis experiments and the absorption measurements (see above) were 0.36 and 0.26, giving EEE fractions of 0.64 and 0.74, respectively. The error of these

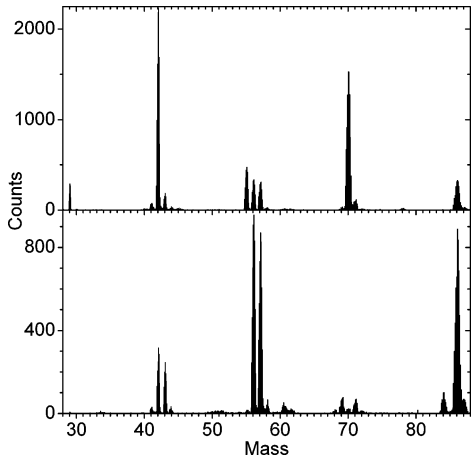

Figure 2. Mass spectra of EEE/hexanes mixture (upper panel, total concentration = 1.45×10^{13} cm^{-3}) and hexanes (lower panel, concentration = 1.12×10^{13} cm^{-3}).

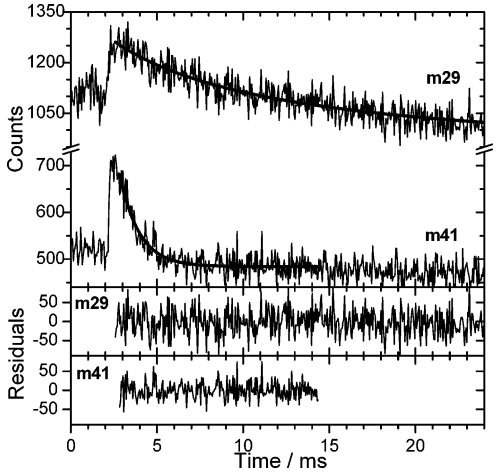

Figure 3. Experimentally observed traces for ethyl (mass 29) and ketenyl (mass 41) radicals as well as fits to the data (heavy lines) and their residuals (lower two panels). Experimental conditions and initial concentrations (in cm^{-3}): T= 298 K, P = 4 Torr, [EEE] = 6.04×10^{12}, Δ[EEE] = 7.92×10^{11}.

fractions was estimated to be less than 10%. By comparison, the original EEE/hexanes sample consisted of about 56% hexanes.

Figure 3 displays a typical example of the signal traces acquired in the photolysis experiments of EEE. Surprisingly, the C_2H_5 and HCCO decays are strikingly different. The kinetics for the ethyl radicals can be understood as radical−radical reactions under conditions of small radical concentrations. In contrast, the "fast" kinetics of the HCCO decays (half-life about 2 ms) was essentially independent of the radical or precursor concentration in the reactor, which leaves only wall reactions as a possible loss mechanism for the disappearance of ketenyl radicals. The traces at masses 26, 28, and those ascribed to EEE (masses 55 and 70) showed the typical increase or drop associated with the photolysis event (see Figure 4). The fast rise of the mass 26 and 28 traces (fitting the mass 26 traces with a simple exponential rise function leads to rates that were at least four times as fast as the decay constants of the HCCO profiles) indicates that the formation of these species is not connected with the loss of HCCO radicals. Therefore, signals at masses 26 and 28 were attributed to acetylene and ethylene, respectively. Moreover, mass spectra taken of neat samples of C_2H_4 showed that the acetylene signal at mass 26 is free of interference from ethylene. Another indicator for the production

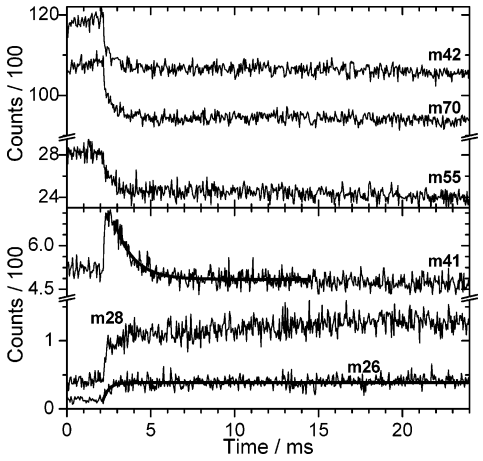

Figure 4. Experimentally observed traces at masses 55 and 70, which were attributed to EEE, mass 42, which had two origins: EEE (94%) and hexanes (6%), and masses 26, 28, and 41, which were attributed to photolysis products acetylene, ethylene, and ketenyl radicals, respectively. Experimental conditions and initial concentrations are the same as in Figure 3. The heavy lines in the lower panel are fits to the data (see text).

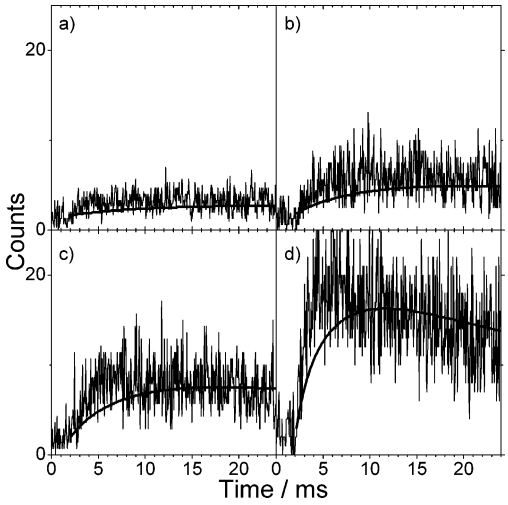

Figure 5. Experimentally observed CH_3 traces following the photolysis of ethyl ethynyl ether. The amount of EEE photolyzed was (in 10^{11} cm^{-3}): (a) 1.74, (b) 3.23, (c) 5.35, and (d) 10.8. The counts are normalized for number of mass spectra acquired and lamp intensity. The heavy lines are simulation calculations. The maximum of the CH_3 trace in panel (d) corresponds to a concentration of about 2×10^{11} cm^{-3}.

of ethylene is the formation of methyl radicals (see Figure 5). The most likely source of methyl radicals is the fast reaction of ethyl radicals with hydrogen atoms,[21] which were generated along with ethylene (channel R1c). Kinetic behavior and yield of the methyl radicals correlate fairly well with the ethyl radical and ethylene concentration. A better fit can be achieved by choosing a higher rate constant for the H + C_2H_5 reaction. With the help of reference measurements, ethylene and acetylene could be quantified. Having determined the EEE contents of the mixtures prepared, the drop of the EEE signal in the photolysis experiments could be directly converted into concentration.

Because C_2H_5 and HCCO radicals were the major products of the EEE photolysis, either ethyl or ketenyl radicals had to be calibrated. For this work, C_2H_5 was calibrated against the concentration of ethyl radicals generated in the photolysis of 3-pentanone. Slagle et al. showed that the photolysis of 3-pentanone at 193 nm and 299 K has three product channels:

$2C_2H_5 + CO$ (69%), $CH_3 + CH_2COC_2H_5$ (13%), and $C_2H_4 + HCOC_2H_5$ (18%).[22] While the methyl signal obtained in this work was too small to be analyzed, the increase in the signal observed at mass 28 was attributed to ethylene (the sensitivity toward CO with H_2 as discharge gas was so small that it had a negligible effect on mass 28) and compared to the drop in the 3-pentanone precursor concentration, giving a yield of 17%, which agrees very well with the value of Slagle et al. The main ion fragments produced in the ionization of ethyl radicals (ionization potential 8.1 eV) in this experiment are vinyl radicals (C_2H_3) at mass 27, which have an appearance potential of 8.25 eV.[23] Significant fragmentation into ethylene ions (appearance potential is about 12 eV. The approximate value was calculated using the heats of formation of the neutral species and the ionization potential of ethylene, 10.5 eV)[23] could be problematic with respect to quantifying ethylene concentrations in the reactor tube. However, the signal at mass 28 showed no time dependence, which, in contrast, was clearly observed for ethyl radicals at masses 27 and 29. Moreover, the relatively high appearance potential for ethylene ions and the excellent agreement between Slagle's ethylene yield and that of this work suggest that fragmentation of ethyl ions into ethylene ions is not significant. A modified second-order decay profile (incorporating first- and second-order loss mechanisms) was fit to the ethyl signal at mass 29.

$$\frac{A_t}{A_0} = \exp(-\kappa_{\text{first}} t) \times \left[\frac{k_{\text{first}}}{2k_{\text{second}}(1 - \exp(-k_{\text{first}} t)) + k_{\text{first}}}\right]^R$$

This equation was adopted from an earlier paper describing the decay of the methylene radical concentration in the presence of excess methyl radicals; k_{first} and κ_{first} are apparent first-order losses of the two radical species.[24] The fits covered only data acquired at least 0.5 ms after the laser was fired. This was necessary because of an inherent finite rise time in every signal. Extrapolating the fit to time zero (synonymous to determining A_0) then gave the initial counts, from which the calibration for the ethyl radical signals could be obtained by comparison with the drop in the precursor concentration with the appropriate photolysis yield. The same procedure was employed to fit the ethyl and ketenyl profiles in the EEE experiments (see Figure 3) as well as the methylene and methyl profiles in the ketene experiments. Usually, all parameters (A_0, k_{first}, κ_{first}, k_{second}, and R) were adjusted independently; however, the ethyl radical profiles closely followed a second-order decay ($k_{\text{first}} \approx \kappa_{\text{first}} \approx 0$, $R \approx 1$), whereas the HCCO profiles could be described by a first-order decay ($k_{\text{second}} \approx 0$). The residuals in Figure 3 indicate that the equation above is able to describe the two very different decay profiles extremely well.

Interestingly, the drop in signal at mass 42, even after subtraction of the hexanes contribution, was always less than those in masses 55 and 70 belonging to EEE. The small difference was attributed tentatively to ketene formed via channel R1b.

Final results are shown in Figure 6, in which concentrations obtained from extrapolations or simple averaging of the experimental data were plotted against the absolute drop in EEE precursor concentration. Straight lines with intercepts fixed to the origin were then fitted to the data points. Linear least-squares analysis leads to the following photolysis yields for each species (slopes) and their errors: $\Phi(C_2H_5) = 0.72 \pm 0.02$, $\Phi(C_2H_4) = 0.32 \pm 0.02$, $\Phi(C_2H_2) = 0.08 \pm 0.01$, and $\Phi(CH_2CO) = 0.015 \pm 0.002$, adding up to a total yield of $\Phi(\text{total}) = \Phi(C_2H_5) + \Phi(C_2H_4) + \Phi(C_2H_2) = 1.12 \pm 0.03$ (keep in mind that $\Phi(CH_2CO)$ is already incorporated in $\Phi(C_2H_4)$). However, the main source of error has been neglected in this treatment, which is the uncertainty in the calibration constants, which is on the order of 20%. Renormalizing the yields and adopting a 20% calibration error for all channels leads to the following yields for the individual channels of reaction R1 at 300 K and 4 Torr helium:

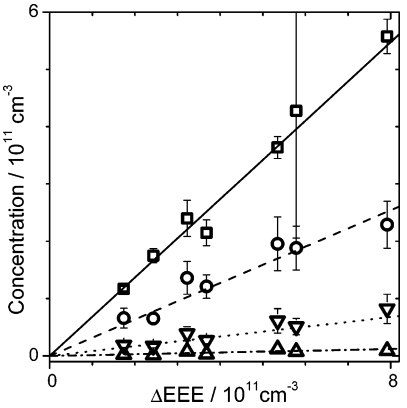

Figure 6. Initial concentrations of C_2H_5 (square), C_2H_4 (circle), CH_2CO (upward-pointing triangle), and C_2H_2 (downward-pointing triangle) as a function of the drop in ethyl ethynyl ether concentration. The lines are error-weighted fits to the data points, for which the intersections were forced through the origin.

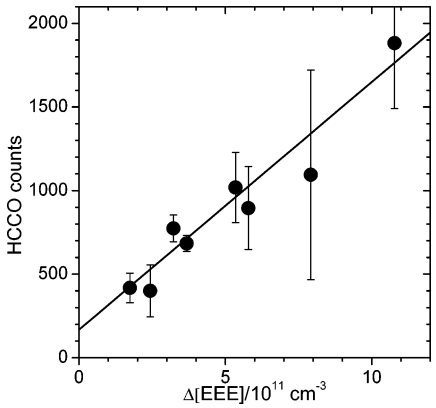

Figure 7. Extrapolated HCCO counts as a function of the drop in ethyl ethynyl ether concentration. The line is an error-weighted fit to the data, giving a calibration constant of (1.6 ± 0.4) counts per (10^9 molecules cm^{-3}) per 100k sweeps per unit lamp intensity.

$$\Phi(\text{R1a}) = 0.64 \pm 0.13$$

$$\Phi(\text{R1b}) = 0.013 \pm 0.003$$

$$\Phi(\text{R1c}) = 0.27 \pm 0.06$$

$$\Phi(\text{R1d}) = 0.071 \pm 0.015$$

This gives a combined yield for the HCCO-producing channels of $\Phi(\text{HCCO}) = 0.91 \pm 0.14$. Finally, from a plot of initial counts at mass 41 against the drop of EEE precursor (see Figure 7), the calibration constant of HCCO radicals can be obtained, which was then used to calibrate the mass 41 signals in the ketene photolysis experiments.

To check whether some of the observed products originate from EEE or hexanes, an EEE/hexanes mixture was prepared with a higher concentration of hexanes (about 70%). The photolytic production of all species scaled with the concentration of EEE and not with that of hexanes. Therefore, contributions of hexanes to the photolysis products can be ruled out.

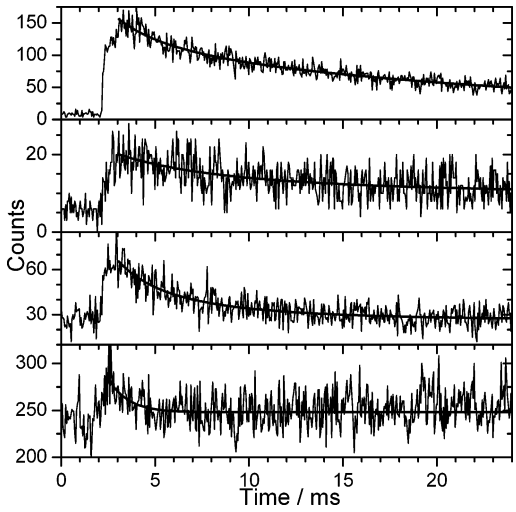

Figure 8. Experimentally observed traces at masses 16 ($^{13}CH_3$, top panel), 15 (CH_3, second panel), 14 ($^3CH_2$, third panel), and 41 (HCCO, lower panel) for the photolysis of ketene. Experimental conditions and initial concentrations (in cm^{-3}): T= 306 K, P = 4 Torr, $[H_2] = 7.71 \times 10^{14}$, [Ketene] = 1.67×10^{13}, [^{13}C-acetone] = 5.15×10^{12}; 8.2% of the acetone and 2.6% of ketene was photolyzed. The heavy lines are fits to the data.

Scavenging of HCCO radicals was also attempted by replacing helium with hydrogen or deuterium as bath gas. Extending the Arrhenius expression for the rate constant of the HCCO + H_2 reaction published recently by Carl et al.[3] to 300 K gave a rate constant of 2.8×10^{-14} cm^3/s, so that a H_2 concentration of 1.2×10^{17} cm^{-3} should have been sufficiently high to capture almost 90% of the HCCO radicals produced. However, no difference in the kinetics could be detected in the mass 41 traces between measurements in helium or H_2/D_2. The most likely explanation for this observation is that the Arrhenius expression cannot be extended to lower temperatures reliably. Also, the product distribution seems not to be influenced by either H_2 or D_2.

Ketene Photolysis. In all experiments, ketene and acetone or 1,3-^{13}C-acetone were photolyzed simultaneously. For the analysis, the ketene signal was referenced to acetone, and methylene and methyl radicals formed in reactions with hydrogen or helium bath gas were referenced to methyl radicals generated in the photolysis of acetone. This was done because increasing concentrations of H_2 in the bath gas also increased the detection sensitivity of each species. Unfortunately, this observation was difficult to describe in detail theoretically because, under the conditions used here, the beam source is characterized somewhere in the transition region between an effusive beam source and supersonic expansion, for which detailed theoretical descriptions are available.[25,26] However, general expressions for the total flow through the orifice indicate that the throughput increases with decreasing viscosity, as seen here, and rising pressure, which was observed in earlier work.[27]

Figure 8 shows a typical example of methylene and methyl signals acquired in the experiments and their fit curves. The same function that was used in the EEE photolysis to describe the ethyl and ketenyl profiles (see above) is employed here in the fit of the methylene and methyl traces. Again, extrapolating the fits to time zero gave the initial signals.

Products of the acetone photolysis at 193 nm have been studied before.[24,28] Primary photolysis of acetone and secondary photolysis of methyl radicals lead to an average effective yield of (96 ± 2)% for channel R3a under the conditions used here. Two to four percent of the primary methyl radicals underwent photodissociation in the same laser pulse, giving methylene radicals and hydrogen atoms.

$$CH_3COCH_3 + h\nu \rightarrow 2CH_3 + CO \quad \text{(R3a)}$$

$$\rightarrow CH_2CO + CH_4 \quad \text{(R3b)}$$

$$CH_3 + h\nu \rightarrow CH_2 + H \quad \text{(R3c)}$$

Because He and H_2/D_2 concentrations are much larger than the concentration of any other species, singlet methylene radicals are converted within less than 10 μs to triplet methylene or methyl radicals, according to reactions R4 and R5 or R6.

$$^1CH_2 + He \rightarrow {}^3CH_2 + He \quad \text{(R4)}$$

$$^1CH_2 + H_2 \rightarrow {}^3CH_2 + H_2 \quad \text{(R5a)}$$

$$\rightarrow CH_3 + H \quad \text{(R5b)}$$

$$^1CH_2 + D_2 \rightarrow {}^3CH_2 + D_2 \quad \text{(R6a)}$$

$$\rightarrow CH_2D + D \quad \text{(R6b)}$$

$$\rightarrow CHD_2 + H \quad \text{(R6c)}$$

Photolysis experiments of ketene in D_2 without acetone showed no signal at mass 15, so that the CH_3 traces in the complete experiments did not have to be corrected for potential secondary chemistry.

In view of the time resolution of the detection system (mass spectra were taken every 48 μs), the $^1CH_2$- to-$^3CH_2/CH_3$ conversion is instantaneous. Therefore, concentrations of species created in the photolysis are identified further on with a "00" subscript, while the initially observed signals are identified with a "0" subscript. Integration of reactions R4 and R5 gives a simple form for the dependence of the initial $^3CH_2$ and CH_3 concentrations on the ratio of reaction rate with H_2 to the total reaction rate:

$$[^3CH_2]_0 = [^3CH_2]_{00} + (1 - f \times X) \times [^1CH_2]_{00}$$

$$[CH_3]_0 = f \times X \times [^1CH_2]_{00}$$

with $X = [H_2]/([H_2] + g \times [He])$, $\quad f = k_{5b}/k_{5a} + k_{5b}$, $\quad g = k_4/(k_{5a} + k_{5b})$.

The values for the factors f (i.e., the relative amount of chemical quenching in the $^1CH_2 + H_2$ reaction) and g (i.e., the ratio of total rate constants of the $^1CH_2 + He$ and $^1CH_2 + H_2$ reactions) can be taken or calculated from literature data to be $f = 0.85 \pm 0.08$ and $g = 0.03$.[29−32]

Using the proper calibration constants, the signals observed can be converted into concentrations, and by normalizing the methylene and methyl concentrations to the amount of ketene photolyzed, the photolysis yields for singlet and triplet methylene can be obtained. As mentioned above, a slightly different approach was used for this study; the ketene concentration was referenced to that of acetone, and the methylene and methyl radicals, whose ultimate source was the photolysis of ketene, were referenced to methyl radicals generated in the photolysis of acetone. The CH_3 reference concentration was obtained from the drop in the acetone concentration. To distinguish the two kinds of methyl radicals, ^{13}C-acetone was used in experiments with H_2, whereas ordinary acetone was used in experiments with D_2. Because the ratios of the calibration constants for ketene to

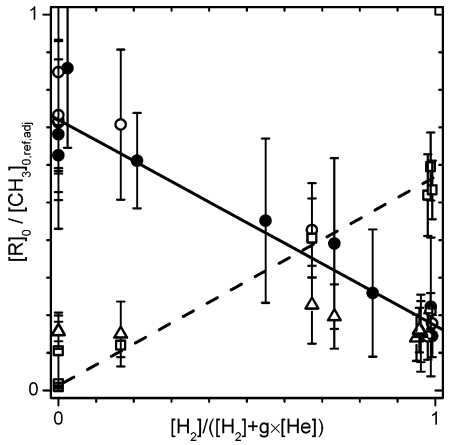

Figure 9. Normalized initial radical concentrations as a function of parameter X (see text) with either H_2 or D_2 as reactant: $^3CH_2$ (open circle) in H_2, $^3CH_2$ (filled circle) in D_2, CH_3 (square) in H_2, and HCCO (triangle). The solid line is a fit to all methylene data, the dashed line is a fit to methyl data.

acetone and $^3CH_2$ to CH_3 to $^{13}CH_3$ are known from this and previous studies, this provides an automatic on-line calibration. Because the experimental CH_3 reference concentration is not the same as the relevant drop in the ketene concentration, the difference between these quantities had to be factored into the final, adjusted CH_3 reference concentration so that $[CH_3]_{0,ref,adj} = [\Delta Ketene]$. This gives the final form for the $^3CH_2$-to-CH_3 dependence on X, with concentrations replaced by $[CH_2]_{00}$ to $[CH_3]_{0,ref,adj}$ ratios, which are the desired photolysis yields:

$$[^3CH_2]_0/[CH_3]_{0,ref,adj} = [^3CH_2]_{00}/[CH_3]_{0,ref,adj} + (1 - f \times X) \times [^1CH_2]_{00}/[CH_3]_{0,ref,adj}$$

$$[CH_3]_0/[CH_3]_{0,ref,adj} = f \times X \times [^1CH_2]_{00}/[CH_3]_{0,ref,adj}$$

As can be seen in Figure 9, the initial triplet methylene and methyl radical concentrations observed follow the anticipated linear relationship with variable X. The absolute values for the slopes ($f \times [^1CH_2]_{00}/[CH_3]_{0,ref,adj}$) of the methylene ($0.55 \pm 0.06$) and methyl ($0.56 \pm 0.05$) points agree very well with each other. The methylene signal evaluated at $X = 0$ gives the total yield for triplet and singlet methylene ($([^3CH_2]_{00} + [^1CH_2]_{00})/[CH_3]_{0,ref,adj} = 0.72 \pm 0.05$). Combining the two results with $f = 0.85$ gives the following photolysis yields for singlet and triplet methylene:

$$\Phi(\text{R2b}) = 0.66 \pm 0.08$$
$$\Phi(\text{R2c}) = 0.06 \pm 0.08$$

Unfortunately, CH_2D and CD_2H data could not be used in the analysis because their calibration constants were not known. Assuming that the calibration constants for both deuterated methyl radicals are similar to the one for CH_3 leads to total methylene yields larger than unity. Therefore, these data were neglected.

In addition, a small signal at mass 41 was observed, which showed the same fast kinetics as was observed in the EEE photolysis experiments (see Figure 8). The signals were attributed to HCCO radicals and were fit in the same way as explained before. Using the calibration constant obtained in the EEE study (see Figure 7), the initial counts were converted into concentrations and divided by the drop in ketene precursor concentration. This resulted in a HCCO yield of:

$$\Phi(\text{R2d}) = 0.17 \pm 0.07$$

Signals at mass 40 (C_2O) could not be detected. Unfortunately, the ionization threshold or cross section of C_2O has not been measured directly, but theoretical calculations and ion−molecule reaction studies indicate that the ionization energies of C_2O or the isoelectronic CNN are below 11 eV,[33−35] which is well within the range of the H_2 emission (ethane has an IP of 11.5 eV[23] and is readily detected by this experiment). Therefore, the absence of the C_2O signal suggests that its concentration is very low, but definite statements about its existence cannot be made here.

Simulation Calculations for Ketene Photolysis. In addition to the analysis of the initial methylene and methyl signals, concentration profiles for reactants as well as products were calculated using the Chemkin II program package.[36] The reaction mechanism is summarized in Tables 2−4. The calculated concentration profiles were converted into counts by multiplication with appropriate calibration constants and fragmentation patterns, which were obtained in separate experiments, with the exception of vinyl radicals, whose calibration constant was chosen to be the same as the one for ethyl radicals (see EEE experiment). Vinyl radicals were generated mainly in the reaction of CH radicals with ketene. As mentioned before, the detection sensitivity increased with increasing hydrogen concentration, which was noticeable in experiments with hydrogen-to-helium ratios of larger than 0.1. The calibration measurements, however, were carried out with helium as bath gas. Therefore, to account for differences in sensitivity, the calibration constants for C2 species were changed according to the increase in counts observed for acetone, whereas the calibration for C1 species was adjusted according to the methyl radical reference signal. The adjustment for C1 species was up to 30% higher than that for the C2 species. The bath gas-dependent detection sensitivity has been discussed above. Unfortunately, the different increases in sensitivity between methyl and methylene radicals on one side and heavier species on the other could not be explained. However, larger signals for CH_3 and CH_2 radicals based on errors in determining their concentrations could be ruled out. In the end, this observation was simply taken as experimental reality.

The simulated signal profiles were then compared to data acquired with a focus on masses 14−16 and 26−32, which covered all reactant and product species. The initial concentrations were determined as outlined above, including the photolysis yields of this work. For the methylene and methyl species, the general agreement between experiment and simulation is very satisfactory, confirming the photolysis yields determined in this work (see Figures 10 and 11). Only at large H_2 concentrations ($> 5 \times 10^{16}$ cm^{-3}) do the simulations predict smaller signals for mass 29 than observed. Adding C_2O as the photolysis product to the initial concentrations had little effect on any mass trace. Also, it has to be mentioned that two adjustments in the reaction mechanism were necessary to obtain good fits for masses 26 (C_2H_2) and 27 (C_2H_3): first, the methylene self-reaction rate constant had to be raised to 1.5×10^{-10} cm^3/s from 5.3×10^{-11} cm^3/s recommended by Baulch et al.[37] This change was advocated earlier by Glass et al. and references therein. Second, the CH + CH_2CO reaction was chosen to yield C_2H_3 + CO (60%) and C_2H_2 + H + CO (40%). This is in contrast to Frey and Walsh, who recommended 15% for the vinyl and 85% for the acetylene channel, which is quite different from an earlier publication from the same group of 65% vinyl and 35% acetylene.[38] Because the product ratio of this work depends on the assumed calibration constant for vinyl radicals, the product distribution of this reaction can only be

TABLE 2: Reaction Mechanism for the Ketene/^{13}C-acetone Photolysis: Bimolecular Reactions[a]

reactions	A	β	E_a	references/comments
$CH + H_2 \rightarrow CH_2 + H$	1.867×10^{14}	0	3279	50
$CH + CH_3 \rightarrow C_2H_3 + H$	6×10^{13}	0	0	assumed
$CH + C_2H_3 \rightarrow CH_2 + C_2H_2$	6×10^{13}	0	0	assumed
$CH + CH_2CO \rightarrow C_2H_2 + CO + H$	5.8×10^{13}	0	0	total rate: 51
$CH + CH_2CO \rightarrow C_2H_3 + CO$	8.6×10^{13}	0	0	see also 38
$CH + CH_3COCH_3 \rightarrow C_2H_4 + CH_3CO$	1.2×10^{14}	0	0	same as $CH + CH_2CO$
$CH_2(S) + He \rightarrow CH_2 + He$	6.624×10^{12}	0	755	32, 52
$CH_2(S) + H_2 \rightarrow CH_2 + H_2$	9.03×10^{12}	0	0	rate: 31, 52
$CH_2(S) + H_2 \rightarrow CH_3 + H$	5.119×10^{13}	0	0	yield: 29
$CH_2(S) + CH_2CO \rightarrow C_2H_4 + CO$	7.838×10^{14}	−0.33	0	31
$CH_2(S) + CH_3COCH_3 \rightarrow C_2H_5 + CH_3CO$	7.838×10^{14}	−0.33	0	same as above
$CH_2 + H \rightarrow CH + H_2$	7.8×10^{12}	0	−1788	20% higher than 53
$CH_2 + CH_2 \rightarrow C_2H_2 + H + H$	9×10^{13}	0	0	this work
$CH_2 + CH_3 \rightarrow C_2H_4 + H$	1.144×10^{14}	0	0	24
$CH_2 + HCCO \rightarrow C_2H_3 + CO$	6×10^{13}	0	0	assumed
$CH_2 + C_2H_3 \rightarrow CH_3 + C_2H_2$	6×10^{13}	0	0	assumed
$C_2H_3 + H \rightarrow H_2 + C_2H_2$	1.2×10^{14}	0	0	assumed
$C_2H_3 + CH_3 \rightarrow CH_4 + C_2H_2$	9×10^{12}	0	765	54
$C_2H_3 + CH_3 \rightarrow C_3H_6$	1.98×10^{13}	0	469	54
$C_2H_3 + C_2H_3 \rightarrow C_2H_2 + C_2H_4$	6×10^{13}	0	0	assumed
$C_2O + H \rightarrow CH + CO$	1.8×10^{13}	0	0	rate: 55
$C_2O + H_2 \rightarrow HCCO + H$	4.2×10^{11}	0	0	rate: 55
$HCCO + H \rightarrow CH_2 + CO$	1.2×10^{14}	0	0	assumed
$HCCO + CH_3 \rightarrow C_2H_4 + CO$	6×10^{13}	0	0	assumed
$C_2H_4 + H \leftrightarrow C_2H_3 + H_2$	1.325×10^{6}	2.53	12240	56
$CH_2CO + H \rightarrow CH_3 + CO$	4.2×10^{10}	0	0	57

[a] Data are given in Chemkin II format: $k = A\,T^{\beta}\exp(-E_a/RT)$ with A in mol cm^3/s, T in K, and E_a in cal/mol.. Reactions of ^{13}C species are not shown, however, they were incorporated into the mechanism by duplicating the appropriate reactions shown in this Table.

TABLE 3: Reaction Mechanism for the Ketene/^{13}C-acetone Photolysis: Pressure-Dependent Reactions[a]

reaction	A	β	E_a	references/comments
$CH+H_2 (+M) \leftrightarrow CH_3 (+M)$	1.970×10^{12}	0.43	−370	56
LOW/4.820×10^{25} −2.80 590.0/				
TROE/0.578 122.0 2535.0 9365.0/				
$CH_3 + H (+M) \leftrightarrow CH_4 (+M)$	2.108×10^{14}	0	0	53
LOW/6.528×10^{23} −1.80 0.00/				
TROE/0.63 61.00 3315.00/				
$CH_3 + CH_3 (+He, H_2) \rightarrow C_2H_6 (+He, H_2)$	He: 2.500×10^{15}, H_2: 2.800×10^{15}	−0.69	175	27, 10% higher A_∞
LOW/8.05×10^{31} −3.75 981.62/				
TROE/0.00 570.00 1000.00/				
$C_2H_4 + H (+M) \rightarrow C_2H_5 (+M)$	3.974×10^{9}	1.28	1292	53
LOW/4.714×10^{18} 0.00 760.00/				
TROE/0.76 40.0 1025/				
$H + C_2H_3 (+M) \rightarrow C_2H_4 (+M)$	6.080×10^{12}	0.27	280	56
LOW/1.400×10^{30} −3.860 3320.00/				
TROE/0.7820 207.50 2663.00 6095.00/				
$H + C_2H_5 (+M) \leftrightarrow C_2H_6 (+M)$	5.210×10^{17}	−0.99	1580	56
LOW/1.990×10^{41} −7.080 6685.00/				
TROE/0.8422 125.00 2219.00 6882.00/				
$CH_3 + C_2H_5 (+M) \leftrightarrow C_3H_8 (+M)$	9.430×10^{12}	0	0	56
LOW/2.710×10^{74} −16.82 13065.0/				
TROE/0.1527 291.0 2742.0 7748.0/				

[a] Reactions involving ^{13}C species are not shown but were added to the mechanism by duplicating reactions shown below. Data are given in Chemkin II format: low and pressure limit rate constants $k = A\,T^{\beta}\exp(-E_a/RT)$ with A_∞ in mol cm^3/s, A_0 in mol^2 cm^6/s, T in K, and E_a in cal/mol. Further information on the format can be found at, e.g., http://www.me.berkeley.edu/gri_mech/data/k_form.html

given with a considerable uncertainty. However, 85% in the acetylene channel would definitely produce too high a signal in mass 26.

4. Discussion

Photolysis of EEE. In general terms, the HCCO yield of 91% found here agrees very well with results of Krisch et al., who investigated the dynamics of the EEE photolysis at 193 nm under high vacuum conditions.[8] However, their product survey did not show any evidence for channels other than C_2H_5 + HCCO (detection of C_2H_4 was not attempted), which can be understood in view of non-HCCO channels being of minor importance (< 8% for acetylene and < 2% for ketene). Acetylene had to be included into the primary photolysis

TABLE 4: Reaction Mechanism for the Ketene/^{13}C-acetone Photolysis: Unimolecular and Wall Reactions[a]

reaction	A	β	E_a	references/comments
$H \rightarrow$ WALL	40	0	0	assumed
$CH \rightarrow$ WALL	40	0	0	assumed
$CH_2 \rightarrow$ WALL	40	0	0	this work
$CH_2(S) \rightarrow$ WALL	500	0	0	same as HCCO loss
$C_2H_3 \rightarrow$ WALL	40	0	0	same as CH_2 loss
$HCCO \rightarrow$ WALL	500	0	0	this work

[a] Data are given in Chemkin II format: $k = A\,T^{\beta}\exp(-E_a/RT)$ with A in s^{-1}, T in K, and E_a in cal/mol.

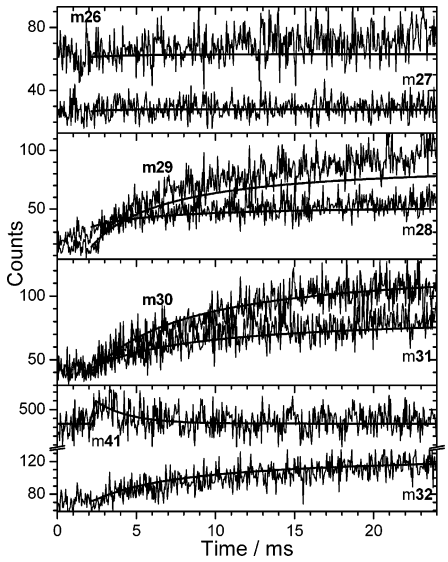

Figure 10. Experimentally observed traces at various masses in the photolysis of ketene. Traces at mass pairs 30/32 and 29/31 were associated mainly with $^{13}C_2H_6$ and $^{13}CH_3CH_3$, while traces at masses 26, 27, 28, and 41 were attributed mainly to C_2H_2, C_2H_3, C_2H_4, and HCCO, respectively. Experimental conditions and initial concentrations (in cm^{-3}): $T = 303$ K, $P = 4$ Torr, $[H_2] = 7.82 \times 10^{16}$, [Ketene] $= 1.48 \times 10^{13}$, [^{13}C-acetone] $= 4.52 \times 10^{12}$; 6.3% of the acetone and 2.4% of ketene was photolyzed. The heavy lines are fits to the data.

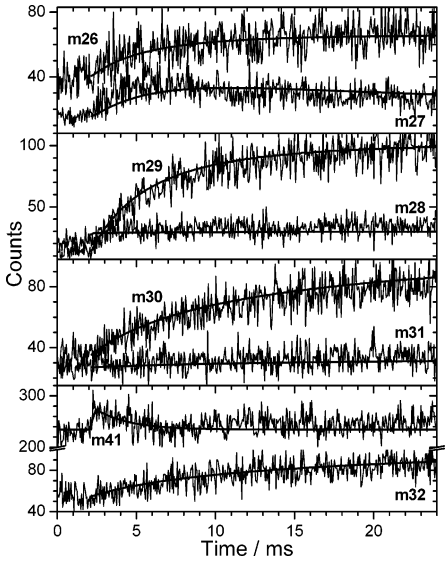

Figure 11. Experimentally observed traces at various masses in the photolysis of ketene. Traces at the mass pair 30/32 was associated mainly with $^{13}C_2H_6$, while traces at masses 26, 27, 28, 29, and 41 were attributed mainly to C_2H_2, C_2H_3, C_2H_4, $^{13}CH_2CH_2$, and HCCO, respectively. Experimental conditions and initial concentrations (in cm^{-3}): $T = 306$ K, $P = 4$ Torr, $[H_2] = 0$, [Ketene] $= 1.39 \times 10^{13}$, [^{13}C-acetone] $= 4.48 \times 10^{12}$; 8% of the acetone and 2.4% of ketene was photolyzed. The heavy lines are fits to the data.

products because the fast rise time of the signal is only consistent if C_2H_2 is a primary photolysis product. Gas-phase reactions can be ruled out as a possible source because the production kinetics of C_2H_2 is too fast for the radical concentrations present in the reactor tube, also too fast in comparison with the disappearance kinetics of HCCO radicals, which is the only probable reactant that could produce acetylene in heterogeneous reactions on the reactor wall. Unfortunately, the attempt to capture HCCO radicals by replacing helium with hydrogen failed (see above), which might have shed more light on the possibility of ketenyl radicals being the origin of secondary products.

From the kinetic energy release of the fragments and additional LIF studies, Krisch et al. concluded that the HCCO fragment is not only vibrationally but also electronically excited. Three electronic states are energetically accessible (ã ^{4}A″, $\tilde{X}$ ^{2}A″, and $\tilde{A}$ ^{2}A′). Because the $\tilde{X}$ and $\tilde{A}$ states (denoted by Krisch et al. as the fast channel) are separated by about 3 kcal/mol, only their combined yield was given with 37%. HCCO in the ã state (denoted as slow channel) was found to have a yield of 63%. Relative ionization cross sections were measured of HCCO in the slow channel compared to HCCO in the fast channel at 10.3 and 11.3 eV. The ionization cross sections of HCCO (ã ^{4}A″) were found to be smaller by a factor of about 2 compared to the fast-channel HCCO. This could have a direct impact on results obtained here if electronically excited HCCO radicals were not deactivated quickly, in which case, the calibration constant found for HCCO radicals would be too low. Furthermore, the determination of the yield of HCCO radicals in the ketene photolysis depends inversely on the calibration constant, and as a consequence, a lower calibration constant would overestimate the production of ketenyl radicals. However, the HCCO yield obtained for the ketene photolysis agrees well with literature data, so that the neglect of two electronic states of HCCO seems to be justified here. In the worst case, the value given for the HCCO yield can be viewed as upper limit.

Krisch et al. also determined that energy between 100 and 355 kJ/mol is partitioned into the internal energy of the HCCO ($\tilde{X}$, $\tilde{A}$) and C_2H_5 fragments and less than 170 kJ/mol in the case of HCCO (ã) + C_2H_5. With about 155 kJ/mol necessary to dissociate ethyl radicals into ethylene and hydrogen atoms, it is quite possible that C_2H_4 is produced in the subsequent dissociation of vibrationally excited C_2H_5, which would have been generated along with HCCO ($\tilde{X}$, $\tilde{A}$). However, an ethylene yield of 27% determined here compared to a 37% yield for the two lowest doublet states of HCCO reported by Krisch et al. indicates that almost all of the ethyl radicals originating from this channel would have to dissociate, which seems unlikely. Alternatively, channel R1b leaves over 680 kJ/mol in the products, ethylene, and ketene. However, excited ketene would most likely dissociate into CH_2 and CO and not into H + HCCO if it were not stabilized. The small ketene yield and the virtual absence of a methylene signal argue against this possibility. Therefore, a direct dissociation of EEE into three species (H, C_2H_4, and HCCO) or via a different, unidentified route cannot be ruled out.

Photolysis of Ketene. Methylene along with CO is the major product, (72 ± 11)%, of the 193-nm photolysis of ketene. This is in agreement with a yield of 82% given by Glass et al. for singlet and triplet methylene combined.[5] However, the singlet-to-triplet methylene ratio obtained here is about 10:1, almost the opposite of the ratio reported by Glass et al. The main origin of this discrepancy can be explained by the additional production of hydrogen atoms seen in their experiments with Ar as bath gas. The additional hydrogen was attributed to the reaction of electronically excited C_2O with ketene. Alternatively, the self-reaction of two methylene radicals can produce hydrogen atoms,[37] and with methylene concentrations in the 10^{13} cm^{-3} range as reported for their experiments, the kinetic behavior observed would be consistent with this hypothesis. Also, allene mentioned by the authors as the main impurity in the ketene sample in amounts of a few percent might be problematic; allene photolysis also generates H atoms, and with an absorption coefficient about twice as large as that of ketene,[39−41] even a

small allene contamination can generate hydrogen atoms in concentrations that are not negligible compared to those produced in the H + HCCO channel. The (17 ± 7)% yield of this work for HCCO radicals is in excellent agreement with the 17% reported by Rim and Hershberger[4] and is in good agreement with the 10.7% by Glass et al. In general, the findings here that $^1CH_2$ + CO and HCCO + H are the two major channels in the photolysis of ketene compare very well with conclusions by Feltham et al.[12] C_2O was proposed as a minor photolysis product (6−7%) by Glass et al. and Laufer,[42] who measured this yield indirectly by observing H_2, HD, and D_2 in the cophotolysis of CH_2CO and CD_2CO. This value would complement the total yield for channels R2b−d measured here of 0.89 ± 0.13 nicely. Glass et al. argued that electronically excited C_2O was produced, which reacted quickly with H_2, giving H + HCCO. This implies that HCCO yields measured at high H_2 concentrations should be larger than yields determined at low or no H_2 concentrations. However, the HCCO yield (see Figure 9) is independent of the H_2 concentration, casting some doubt on the interpretation of Glass et al. Unfortunately, the sensitivity of this experiment toward C_2O was not known, so that from the lack of any signal at mass 40, its absence cannot be inferred.

The analysis of the EEE and ketene photolysis yields so far neglected any secondary photolysis of HCCO radicals in the same laser pulse. The main photodissociation channel operates via breaking of the C−C bond, producing CO molecules and CH radicals, which were observed after single-photon absorption of HCCO radicals at wavelengths between 208 and 308 nm.[43] Moreover, fluorescence of excited CH radicals was observed after photolysis of ketene at 193 nm and attributed to a two-photon process involving HCCO as intermediate.[44] Unfortunately, this two-photon process has not been measured quantitatively, and therefore, estimates of its influence on the results of this work on the basis of excimer laser fluence cannot be made.

In the analysis of the EEE photolysis experiments, the HCCO yield was determined indirectly from the C_2H_4 and C_2H_6 yields, and therefore, photodissociation of HCCO was not a problem per se. However, a significant HCCO photolysis would be problematic if other C2 species (C_2H_2, C_2H_4, C_2H_5, CH_2CO) were produced in fast reactions of CH radicals with the most abundant species, EEE and, to a lesser extent, hexanes ([EEE]/[hexanes] ≈ 2.5), which also denied any possibility of detecting CH radicals directly. Consequently, experiments in which the hexanes concentration was enriched over the EEE concentration ([hexanes]/[EEE] ≈ 2.5) or in which He was replaced by either H_2 or D_2, were anticipated to scavenge CH radicals and, therefore, should show a difference in the yields if CH radicals were producing C2 species in significant amounts. However, no significant change in the ratio between amounts of photolysis products and the amount of precursor photolyzed could be detected. In the case of H_2 as bath gas, any CH radicals should have been converted to CH_2 or CH_3 in roughly equal amounts under the present conditions. Only a very small signal at mass 14 was detected, which would translate into less than 15% loss of HCCO radicals due to secondary photolysis, if indeed CH radicals were the cause of this signal. In addition, the excimer laser power was varied by a factor of about four, which did not alter the yields. Therefore, it was concluded that effects of the photodissociation of HCCO on the yields measured in the EEE photolysis study were not important.

Secondary photolysis of HCCO in the ketene experiments is more problematic because the HCCO yield relies on the HCCO signal calibration obtained from the EEE experiments. Interestingly, if the magnitude of the photolysis of HCCO radicals in the EEE and ketene experiments were the same, the errors induced by a wrong calibration coefficient would cancel each other, giving the correct value for the HCCO yield. Also, CH radicals can produce additional methylene and methyl radicals in reactions with H_2. As a consequence, the methyl and methylene concentrations at high H_2 concentrations would be larger with HCCO photolysis than without, while their concentrations at low H_2 concentrations would remain unchanged (CH radicals would react predominantly with ketene, producing acetylene and vinyl radicals). Consequently, the slopes of the normalized methyl and methylene concentrations as a function of parameter X (the absolute values should be equal, see Figure 9) should differ significantly, which, however, was not observed. In addition, if CH radicals were produced from HCCO, then the initial $^3CH_2$ concentrations observed in experiments using D_2 should be smaller than the concentrations found in H_2 experiments because the CH + D_2 reaction would not produce any interfering CH_2. Again, no evidence for this behavior was found (see, e.g., CH_2 yield for $X \approx 1$; open and filled circles in Figure 9). Finally, considering a HCCO yield of around 20% and assuming that not more than 15% of the HCCO radicals was photolyzed as discussed above, it is not surprising that evidence of any secondary photodissociation of HCCO radicals would be difficult to detect in the ketene photolysis experiments. In summary, secondary HCCO photolysis cannot be ruled out; however, its influence on the results of this work is not significant.

5. Conclusion

The product distributions of the excimer laser photolysis of ethyl ethynyl ether and ketene at 193.3 nm have been measured. Questions of whether singlet or triplet methylene is produced in the photolysis of ketene could be unambiguously answered: $^1CH_2$ (66 ± 8)% and $^3CH_2$ (6 ± 8)%. Ketenyl radicals as photolysis products could be quantified for both precursors: (17 ± 7)% for ketene and (91 ± 14)% for ethyl ethynyl ether. Moreover, it could be shown that the product distribution of the ethyl ethynyl ether photolysis is more complex than previously thought; not only HCCO and C_2H_5, but also C_2H_4 and C_2H_2 were detected. However, some questions remain that could not be answered with this experiment: is the methylene that is initially produced in the ketene photolysis in the $^1B_1$ or $^1A_1$ state, and is C_2O produced in this process at all? These problems are better addressed by other means such as visible or IR spectroscopic techniques.

Acknowledgment. I would like to thank all of the following current and former group members at the Brookhaven National Laboratory: James Muckerman, Jack Preses, Ralph Weston, Trevor Sears, Gregory Hall, and Hua-Gen Yu. I also thank one reviewer of this paper for suggestions regarding the discussion of the results. This work was carried out at Brookhaven National Laboratory under Contract DE-AC02-98CH10886 with the U.S. Department of Energy and supported by its Division of Chemical Sciences, Office of Basic Energy Sciences.

References and Notes

(1) Miller, J. A.; Kee, R. J.; Westbrook, C. K. *Annu. Rev. Phys. Chem.* **1990**, *41*, 345.

(2) Miller, J. A.; Klippenstein, S. J.; Glarborg, P. *Combust. Flame* **2003**, *135*, 357.

(3) Carl, S. A.; Sun, Q.; Teugels, L.; Peeters, J. *Phys. Chem. Chem. Phys.* **2003**, *5*, 5424.

(4) Rim, K. T.; Hershberger, J. F. *J. Phys. Chem. A* **2000**, *104*, 293.
(5) Glass, G. P.; Kumaran, S. S.; Michael, J. V. *J. Phys. Chem. A* **2000**, *104*, 8360.
(6) Osborn, D. L. *J. Phys. Chem. A* **2003**, *107*, 3728.
(7) Alvarez, R. R.; Moore, C. B. *J. Phys. Chem.* **1994**, *98*, 174.
(8) Krisch, M. J.; Miller, J. L.; Butler, L. J.; Su, H.; Bersohn, R.; Shu, J. *J. Chem. Phys.* **2003**, *119*, 176.
(9) Allen, W. D.; III, H. F. S. *J. Chem. Phys.* **1988**, *89*, 329.
(10) Liu, X.; Westre, S. G.; Getty, J. D.; Kelly, P. B. *Chem. Phys. Lett.* **1992**, *188*, 42.
(11) Ruiz, J.; Martín, M. *Chem. Phys. Lett.* **1994**, *226*, 300.
(12) Feltham, E. J.; Qadiri, R. H.; Cottrill, E. E. H.; Cook, P. A.; Cole, J. P.; Balint-Kurti, G. G.; Ashfold, M. N. R. *J. Chem. Phys.* **2003**, *119*, 6017.
(13) Fujimoto, G. T.; Umstead, M. E.; Lin, M. C. *Chem. Phys.* **1982**, *65*, 197.
(14) Hartland, G. V.; Qin, D.; Dai, H.-L. *J. Chem. Phys.* **1993**, *98*, 6906.
(15) Fockenberg, C.; Bernstein, H. J.; Hall, G. E.; Muckerman, J. T.; Preses, J. M.; Sears, T. J.; Weston, R. E., Jr. *Rev. Sci. Instr.* **1999**, *70*, 3259.
(16) Phillips, L. F. *J. Phys. Chem.* **1981**, *85*, 3994.
(17) Manatt, S. L.; Lane, A. L. *J. Quant. Spectrosc. Radiat. Transfer* **1993**, *50*, 267.
(18) Fockenberg, C.; Weston, R. E., Jr.; Muckerman, J. T. *J. Phys. Chem. B* **2005**, *109*, 8415.
(19) Rudolph, R. N.; North, S., W.; Hall, G. E.; Sears, T. J. *J. Chem. Phys.* **1997**, *106*, 1346.
(20) Berg, O.; Ewing, G. E. *J. Phys. Chem.* **1991**, *95*, 2908.
(21) Pimentel, A. S.; Payne, W. A.; Nesbitt, F. L.; Cody, R. J.; Stief, L. J. *J. Phys. Chem. A* **2004**, *108*, 7204
(22) Slagle, I. R.; Sarzynski, D.; Gutman, D.; Miller, J. A.; Melius, C. F. *J. Chem. Soc., Faraday Trans. 2* **1988**, *84*, 491.
(23) NIST Chemistry WebBook. http://webbook.nist.gov/chemistry, (accessed 2003).
(24) Wang, B.; Fockenberg, C. *J. Phys. Chem. A* **2001**, *105*, 8449.
(25) Miller, D. R. Free Jet Sources. In *Atomic and Molecular Beam Methods*; Scoles, G., Ed.; Oxford University Press: New York, 1988; Vol. 1.
(26) Pauly, H. Other Low-Energy Beam Sources. In *Atomic and Molecular Beam Methods*; Scoles, G., Ed.; Oxford University Press: New York, 1988; Vol. 1.
(27) Wang, B.; Hou, H.; Yoder, L. M.; Muckerman, J. T.; Fockenberg, C. *J. Phys. Chem. A* **2003**, *107*, 11414.
(28) Lightfoot, P. D.; Kirwan, S. P.; Pilling, M. J. *J. Phys. Chem.* **1988**, *92*, 4938.
(29) Blitz, M. A.; Choi, N.; Kovács, T.; Seakins, P. W.; Pilling, M. J. The Effect of Temperature on Collision-Induced Intersystem Crossing in the Reaction of $^1CH_2$ with H_2; Thirtieth Symposium (International) on Combustion, Chicago, IL, 2004.
(30) Blitz, M. A.; Pilling, M. J.; Seakins, P. W. *Phys. Chem. Chem. Phys.* **2001**, *3*, 2241.
(31) Hancock, G.; Heal, M. R. *J. Phys. Chem.* **1992**, *96*, 10316.
(32) Wagener, R. *Z. Naturforsch., A.: Phys. Sci.* **1990**, *45*, 649.
(33) Maclagan, R. G. A. R.; Sudkeaw, P. *J. Chem. Soc., Faraday Trans.* **1993**, *89*, 3325.
(34) Schildcrout, S. M.; Franklin, J. L. *J. Am. Chem. Soc.* **1970**, *92*, 251.
(35) Lu, W.; Tosi, P.; Bassi, D. *J. Chem. Phys.* **2000**, *113*, 4132.
(36) Kee, R. J.; Rupley, F. M.; Miller, J. A. Chemkin-II: A Fortran Chemical Kinetics Package for the Analysis of Gas-Phase Chemical Kinetics; Sandia National Laboratories: Albuquerque, NM, 1996.
(37) Baulch, D. L.; Cobos, C. J.; Cox, R. A.; Esser, C.; Frank, P.; Just, T.; Kerr, J. A.; Pilling, M. J.; Troe, J.; Walker, R. W.; Warnatz, J. *J. Phys. Chem. Ref. Data* **1992**, *21*, 411.
(38) Frey, H. M.; Walsh, R. *J. Phys. Chem.* **1985**, *89*, 2445.
(39) Sun, W.; Yokoyama, K.; Robinson, J. C.; Suits, A. G.; Neumark, D. M. *J. Chem. Phys.* **1999**, *110*, 4363.
(40) Ni, C.-K.; Huang, J. D.; Chen, Y. T.; Kung, A. H.; Jackson, W. M. *J. Chem. Phys.* **1999**, *110*, 3320.
(41) Chen, F. Z.; Judge, D. L.; Wu, C. Y. R. *Chem. Phys.* **2000**, *260*, 215.
(42) Laufer, A. H. *J. Phys. Chem.* **1969**, *73*, 959.
(43) Mordaunt, D. H.; Osborn, D. L.; Choi, H.; Bise, R. T.; Neumark, D. M. *J. Chem. Phys.* **1996**, *105*, 6078.
(44) Carl, S. A.; Sun, Q.; Peeters, J. *J. Chem. Phys.* **2001**, *114*, 10332.
(45) Ruscic, B.; Litorja, M.; Asher, R. L. *J. Phys. Chem. A* **1999**, *103*, 8625
(46) Osborn, D. L.; Mordaunt, D. H.; Choi, H.; Bise, R. T.; Neumark, D. M.; Rohlfing, C. M. *J. Chem.* Phys. **1997**, *106*, 10087.
(47) *NIST-JANAF Themochemical Tables*; 4th ed.; Chase, M. W., Jr., Ed.; American Chemical Society: Washington, DC, 1998; Monograph 9, p 1.
(48) Tsang, W. Heats of Formation of Organic Free Radicals by Kinetic Methods. In *Energetics of Organic Free Radicals*; Simoes, J. A. M., Greenberg, A., Liebman, J. F., Eds.; Blackie Academic and Professional: London, 1996; p 22.
(49) Wiberg, K. B.; Crocker, L. S.; Morgan, K. M. *J. Am. Chem. Soc.* **1991**, *113*, 3447.
(50) Brownsword, R. A.; Canosa, A.; Rowe, B. R.; Sims, I. R.; Smith, I. W. M.; Stewart, D. W. A.; Symonds, A. C.; Travers, D. *J. Chem. Phys.* **1997**, *106*, 7662.
(51) Hancock, G.; Heal, M. R. *J. Chem. Soc., Faraday Trans.* **1992**, *88*, 2121.
(52) Ashfold, M. N. R.; Fullstone, M. A.; Hancock, G.; Ketley, G. W. *Chem. Phys.* **1981**, *55*, 245.
(53) Baulch, D. L.; Cobos, C. J.; Cox, R. A.; Frank, P.; Hayman, G.; Just, T.; Kerr, J. A.; Murrels, T.; Pilling, M. J.; Troe, J.; Walker, R. W.; Warnatz, J. *J. Phys. Chem. Ref. Data* **1994**, *23*, 847.
(54) Stoliarov, S. I.; Knyazev, V. D.; Slagle, I. R. *J. Phys. Chem. A* **2000**, *104*, 9687.
(55) Horie, O.; Bauer, W.; Meuser, R.; Schmidt, V. H.; Becker, K. H. *Chem. Phys. Lett.* **1983**, *100*, 251.
(56) Smith, G. P.; Golden, D. M.; Frenklach, M.; Moriarty, N. W.; Eiteneer, B.; Goldenberg, M.; Bowman, C. T.; Hanson, R. K.; Song, S.; Gardiner, W. C., Jr.; Lissianski, V. V.; Qin, Z. GRI-MECH 3.0; http://www.me.berkeley.edu/gri_mech/, 1999.
(57) Michael, J. V.; Nava, D. F.; Payne, W. A.; Stief, L. J. *J. Chem. Phys.* **1979**, *70*, 5222.